The N-terminal 26-residue fragment of human programmed cell death 5 protein can form a stable α-helix having unique electrostatic potential character

Dongsheng LIU*[1], Hongwei YAO*[1], Yaoyao CHEN†, Yingang FENG*, Yingyu CHEN† and Jinfeng WANG*[2]

*National Laboratory of Biomacromolecules, Center for Molecular Biology, Institute of Biophysics, Chinese Academy of Sciences, 15 Datun Road, Beijing 100101, China, and †Laboratory of Medical Immunology, School of Basic Medical Science, Peking University Health Science Center, 38 Xueyuan Road, Beijing 100083, China

PDCD5-(1–26) is a N-terminal 26-residue fragment of human PDCD5 (programmed cell death 5) protein. PDCD5 is an important novel protein that regulates both apoptotic and non-apoptotic programmed cell death. The conformation of PDCD5 protein is a stable helical core consisting of a triple-helix bundle and two dissociated terminal regions. The N-terminal region is ordered and contains abundant secondary structure. Overexpression and purification of the N-terminal 26-residure fragment, PDCD5-(1–26), was performed in this study to better understand its tertiary structure. The spectroscopic studies using CD and hetero- and homo-nuclear NMR methods determine a stable α-helix formed by Asp^3–Ala^{19} of PDCD5-(1–26). The N-terminal residues Asp^3–Ala^{19} of PDCD5 were then affirmed to have the capacity to form a stable α-helix independently of the core of the protein. Analysis of the helical peptide of PDCD5-(1–26) indicates that the surface of this well-formed α-helix has a unique electrostatic potential character. This may provide an environment for the N-terminal α-helix of PDCD5 to serve as an independent functional entity of the protein. The apoptosis activity assay shows that the deletion of the N-terminal α-helix of PDCD5 significantly attenuates the apoptosis-promoting effects on HL-60 cells induced by serum withdrawal.

Key words: apoptosis, electrostatic potential surface, α-helix, NMR, programmed cell death 5 (PDCD5), solution structure.

INTRODUCTION

PDCD5 (programmed cell death 5) is a protein that is involved in the regulation of cell apoptosis [1]. Studies of the biological activities of the PDCD5 protein have found that PDCD5 is expressed in tumour cells during apoptosis, and the expressed level of PDCD5 is significantly higher than that in normal cells. The expressed PDCD5 protein has been shown to traverse rapidly from the cytoplasm to the nucleus of cells and distribute uniformly in cells that undergo apoptosis [2]. The enhancement of TAJ [toxicity and JNK (c-Jun N-terminal kinase) inducer]/TROY-triggered paraptosis-like cell death by PDCD5 overexpression suggested that PDCD5 is an important regulator not only in apoptotic, but also in non-apoptotic, programmed cell death [3].

The sequence of human PDCD5 shares significant similarity with the corresponding proteins of species ranging from yeast to mice [1,4]. MTH1615 (MTH1615, *Methanobacterium thermoautotrophicum* 1615) is an orthologue of human PDCD5 in a thermophilic archaeon. The three-dimensional solution structure of the protease-resistant domain of MTH1615 protein was determined as a triple-helix bundle. However, the N-terminal 31 residues of MTH1615 protein were found as an unstructured region in solution, although this region was strongly predicted to be an α-helix [5]. In a previous study, we demonstrated that the conformation of human PDCD5 has three structural regions: a rigid core region and two dissociated terminal regions. The secondary chemical shifts and ^{15}N relaxation data collected for PDCD5 by heteronuclear NMR experiments suggested that the N-terminal residues of PDCD5 tend to form a stable α-helical structure [4]. The N-terminal sequence Ser^1–Gly^{22} of PDCD5 has eight amino acids identical with residues in the sequence Met^1–Gln^{20} of MTH1615 (Figure 1). Thus it is interesting to determine experimentally whether the N-terminal residues of PDCD5 form an α-helix independently of the core of the protein. In the present study, we have successfully expressed and purified PDCD5-(1–26), a fragment containing residues 1–26 of PDCD5. The three-dimensional conformation of PDCD5-(1–26) was studied by CD and multidimensional NMR methods. Analysis of the structural features of PDCD5-(1–26) suggests that the N-terminal peptide corresponding to the first 20 residues of PDCD5 can form a stable α-helix independently of the core of the protein. For an investigation of the functional entity of the N-terminal α-helix in PDCD5, an N-terminal-truncated PDCD5 consisting of residues Met^{39}–Tyr^{125}, PDCD5-(39–125), was purified. The apoptosis activity assay of PDCD5-(39–125) and PDCD5 was carried out.

MATERIALS AND METHODS

Expression and purification of PDCD5-(1–26) and PDCD5-(39–125)

For expression of PDCD5-(1–26), the fusion expression system used for expression of the intact human PDCD5 protein [6] was adopted. PDCD5-(1–26) was produced by mutation of Ala^{27} of PDCD5 to a terminator in the expression plasmid pET-3d-HR52-PDCD5 by the QuikChange (Stratagene) method [7]. Two primers, primer 1 (5′-CGGCGATCCTGGTGATTAAGCCCAACAGGAAGCAAAGC-3′) and primer 2 (5′-GCTTTGCTTCCTGTTGGGCTTAATCACCAGGATCGCCG-3′) were used as the

Abbreviations used: HMQC, heteronuclear multiple-quantum correlation; HSQC, heteronuclear single-quantum correlation; MTH1615, *Methanobacterium thermoautotrophicum* 1615; NOE, nuclear Overhauser effect; PDCD5, programmed cell death 5; PS, phosphatidylserine; R.M.S.D., root mean square deviation.

[1] These authors contributed equally to this work.

[2] To whom correspondence should be addressed (email address: jfw@sun5.ibp.ac.cn).

The atomic co-ordinates for PDCD5-(1–26) will appear in the Protein Data Bank under the accession code 1YYB.

Figure 1 Sequence alignment of PDCD5-(1–26) with the N-terminal 29 residues of MTH1615 protein from a thermophilic archaeon [4]

forward and reverse primers respectively. In the expression plasmid, there is a thrombin cleavage site (LVPR↓GS) between the fusion partner HR52, a His_6-tagged N-terminal 52-residue fragment of staphylococcal nuclease R, and a target protein for removing the fusion partner. To purify the HR52–PDCD5-(1–26), a 10 cm × 1 cm column of chelating Sepharose Fast Flow charged with Ni^{2+} was used. The flow rate was 1.0 ml/min. The recovered supernatant containing the overexpressed HR52–PDCD5-(1–26) was loaded on to the column. The column was then washed by the same procedure using the same buffers as described for purification of HR52–PDCD5. The digestion with thrombin (Sigma) was carried out on the column as described in the previous study [4]. The eluate containing PDCD5-(1–26) and thrombin was collected and precipitated by adding a 4-fold volume of cold (−20 °C) ethanol. PDCD5-(1–26) can precipitate fully while the elute is kept overnight in 80 % (v/v) cold ethanol. The precipitate was collected by centrifugation (13 000 ***g*** for 15 min at 4 °C) and dissolved in 5 ml of water. Only PDCD5-(1–26) can refold well and has good solubility in water, since it is a small fragment. The solution was freeze-dried and stored at −20 °C. As a result of thrombin cleavage, residue Met^1 in the sequence of PDCD5 was replaced by Gly^0–Ser^1, and the sequence of PDCD5-(1–26) consists of 27 amino acid residues.

For expression of PDCD5-(39–125), an N-terminal truncated fragment of PDCD5 containing residues Met^{39}–Tyr^{125}, the target gene was amplified from the plasmid pET-3d-HR52-PDCD5 and cloned using the NdeI and BamHI restriction sites of the vector pET-28b (Novagen) to generate expression plasmid pET-28b-PDCD5(39-125). Expression and purification of PDCD5-(39–125) were carried out using a similar method as described in the previous study for isolation of PDCD5 protein [4]. Three residues, Gly-Ser-His, are appended to the N-terminal residue Met^{39} of PDCD5-(39–125) as a result of the thrombin cleavage.

Far-UV CD measurement

The far-UV CD spectrum for PDCD5-(1–26) at concentration of 0.125 mg/ml in 20 mM phosphate buffer (pH 6.5) was recorded on a Jasco 720 spectropolarimeter at room temperature (25 °C). Measurements were carried out with a 1-mm-pathlength cuvette over the wavelength range from 190 to 250 nm at 1 nm bandwidth. Typically, four scans were averaged for the collecting spectrum.

NMR spectroscopy

Samples of uniformly ^{15}N-labelled and unlabelled PDCD5-(1–26) were prepared for NMR studies. PDCD5-(1–26) (2.0–4.0 mM) was dissolved in $H_2O/^2H_2O$ (9:1, v/v) containing 50 mM phosphate buffer (pH 6.5), 200 mM NaCl and 0.01 mM NaN_3.

All NMR spectra were acquired at room temperature on a Bruker DMX 600 spectrometer equipped with a z-gradient triple-resonance cryo-probe. The three-dimensional heteronuclear NMR experiments, ^1H–^{15}N NOESY–HSQC (heteronuclear single-quantum correlation) and TOCSY–HSQC, were performed on 4.0 mM ^{15}N-labelled PDCD5-(1–26) in aqueous solution with mixing times of 200 ms and 70 ms respectively. The two-dimensional ^1H–^{15}N HSQC experiments were recorded on 2.0 mM ^{15}N-labelled PDCD5-(1–26) in aqueous solution. The two-dimensional ^1H–^{13}C HMQC (heteronuclear multiple-quantum correlation), HMQC–NOESY, and HMQC–TOCSY spectra were acquired for 3.0 mM naturally abundant PDCD5-(1–26) in 99.996 % ^2H_2O containing 50 mM phosphate buffer (pH 6.5) and 200 mM NaCl. The two-dimensional homonuclear ^1H NOESY and TOCSY experiments were also carried out for naturally abundant PDCD5-(1–26) in aqueous solution.

The two-dimensional ^1H–^{15}N R_1, R_2 and NOE (nuclear Overhauser effect) spectra were obtained using standard pulse sequences with a water flip-back scheme [8]. ^{15}N R_1 rates were measured by a series of experiments performed with T_1 relaxation periods of 0.02, 0.06, 0.14, 0.24, 0.36, 0.53, 0.76, 1.15 and 1.50 s. ^{15}N R_2 rates were recorded with a CPMG (Carr–Purcell–Meiboom–Gill) spin-echo period of 500 μs, and with T_2 relaxation periods of 17.0, 33.9, 55.9, 67.8, 84.8, 101.8, 118.7, 135.7, 169.6 and 203.5 ms. The ^1H–^{15}N NOE values were collected by two ^1H–^{15}N HSQC experiments. In the NOE experiment, a delay of 2.0 s was followed by ^1H saturation for 3.0 s. In the control experiment, the saturation period was replaced by a delay of equivalent duration (3.0 s). The two experiments were performed in an interleaved manner.

All NMR data were processed and analysed with FELIX98 (MSI/Accelrys). The data points in each indirect dimension were usually doubled by linear prediction before zero filling to the appropriate size [9]. A 70–90° shifted square sine bell apodization was used for all dimensions before Fourier transformation. ^1H chemical shifts were referenced to internal DSS (2,2-dimethyl-2-silapentane-5-sulphonate). ^{15}N and ^{13}C chemical shifts were referenced indirectly [10]. Experimental R_1, R_2 and NOE relaxation values, and the uncertainties associated with these parameters, were obtained by the same procedures as described in [4].

Structure calculation

Based on the main-chain and side-chain resonance assignments, the NOE connectivities were identified for PDCD5-(1–26). The torsion angle restraints for PDCD5-(1–26) were generated with the program TALOS [11]. The structure calculations were carried out on Silicon Graphics station Onyx2 employing the program CNS1.1 [12]. A family of 200 structures was calculated, and the final family consisting of 20 conformers with the lowest target function was selected for structural analysis.

Induction and detection of cell apoptosis

HL-60 cells were cultured in complete medium consisting of RPMI 1640 medium supplemented with 15 % foetal bovine serum. For induction of apoptosis, HL-60 cells were washed twice in medium without serum. After the second wash, cells were resuspended and adjusted to 2×10^5/ml. Cell suspensions were added into 24-well plates (0.5 ml for each well), and then both intact PDCD5 and PDCD5-(39–125) with different amounts (20 and 30 μg) were added to each well. BSA (20 μg) and etoposide (20 μg) were used as negative and positive controls respectively. The cells were harvested after treatment for 20 h and washed twice with PBS, followed by resuspending in 100 μl of annexin-V-binding buffer (10 mM Hepes, 140 mM NaCl, 2 mM $MgCl_2$, 5 mM KCl and 2.5 mM $CaCl_2$, pH 7.4). FITC-conjugated annexin V (10 μl) (Beijing Biosea Biotechnology Co.) was added according to the manufacturer's protocol. After incubation for 20 min at room temperature in the dark, another 400 μl of binding buffer was added, and samples were immediately analysed on

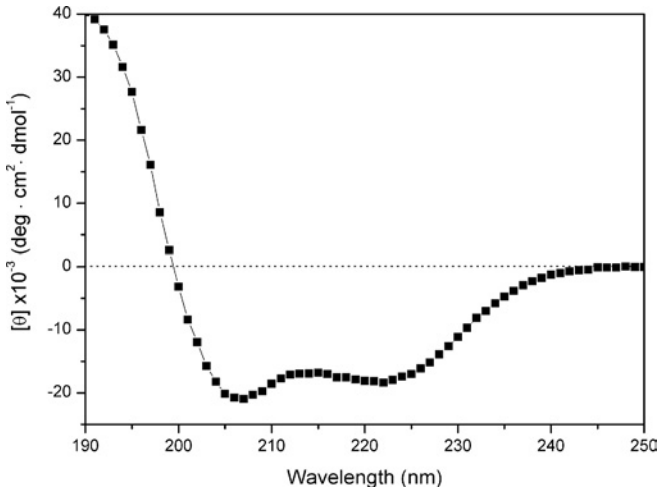

Figure 2 Far-UV CD spectrum of PDCD5-(1–26) in 20 mM phosphate buffer at pH 6.5

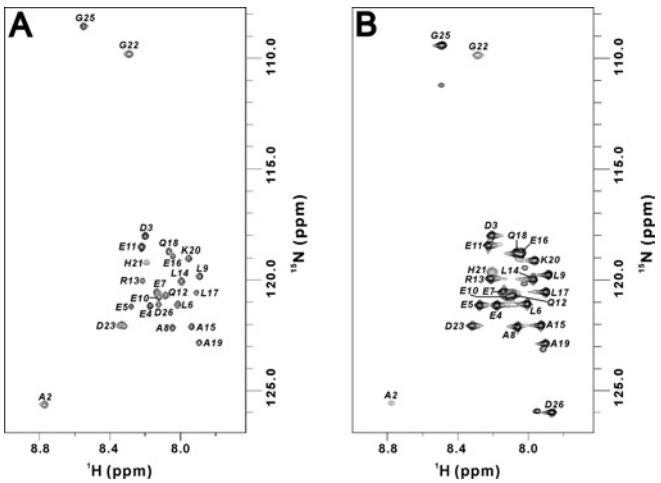

Figure 3 Two-dimensional ^{1}H–^{15}N HSQC spectra of PDCD5-(1–26) (A) and intact human PDCD5 (B)

Only cross-peaks for residues Ser^1–Asp^{26} of PDCD5 show up when the two-dimensional ^{1}H–^{15}N HSQC spectrum of PDCD5 [4] is plotted with high contour levels in (**B**). The assignments of ^1H_N–^{15}N cross-peaks for PDCD5-(1–26) are indicated in (**A**).

a FACSCalibur. Cells (1×10^4) were collected and analysed with CELLQuest software (BD Bioscience). Apoptotic cells are expressed as a percentage of total cells.

RESULTS

Expression and purification of PDCD5-(1–26) and PDCD5-(39–125)

For structural analysis of PDCD5-(1–26), a better signal separation of NMR spectra is necessary for resonance assignments. The most important advantage of the multinuclear and multidimensional NMR experiments is to reduce signal degeneracy in NMR spectra. Stable-isotope-labelled PDCD5-(1–26) is then required for this study. For fulfilling this requirement, the expression plasmid pET-3d-HR52-PDCD5(1-26) with a small fusion partner His_6-tagged HR52 was obtained. Expression and purification of PDCD5-(1–26) in *Escherichia coli* was analysed by 16.5 % tricine SDS/PAGE. The desired recombinant His_6-tagged HR52–PDCD5-(1–26) was highly expressed in soluble form. PDCD5-(1–26) was successfully purified by twice precipitating the collected eluate after digestion with thrombin in 80 % (v/v) cold ethanol and followed by dissolving the precipitate in aqueous solution.

For investigation of the functional entity of the N-terminal α-helix in PDCD5, the N-terminal-truncated PDCD5 is required. PDCD5-(39–125) is a fragment of PDCD5 which was obtained by deletion of the N-terminal α-helix and a segment connecting the α-helix and triple-helix bundle of the protein. PDCD5-(39–125) was purified successfully, and the purification was analysed by following similar procedures as described above.

Secondary structure of PDCD5-(1–26) inferred from the CD spectrum

The far-UV CD spectrum of PDCD5-(1–26) is shown in Figure 2. Two apparent negative minima at 208 and 222 nm of the spectrum in the far-UV region show the presence of a stable helical secondary structure in PDCD5-(1–26). Analysis of the molar ellipticity values for PDCD5-(1–26) using the CONTIN program in the software package CDPro (http://lamar.colostate.edu/∼sreeram/CDPro) provided the estimations of the secondary-structural components: 54.4 % of α-helix, 28.4 % of random coil, 12.6 % of turn and 4.6 % of β-sheet contents in PDCD5-(1–26).

Secondary chemical shifts of PDCD5-(1–26)

Analysis of the acquired heteronuclear NMR spectra provide the ^1H_N and ^{15}N resonance assignments for PDCD5-(1–26). Figure 3(A) shows the two-dimensional ^{1}H–^{15}N HSQC spectrum of PDCD5-(1–26). The dispersion of ^1H_N–^{15}N cross-peaks for residues of PDCD5-(1–26) in Figure 3(A) was highly similar to the distribution of cross-peaks for corresponding residues in PDCD5 (Figure 3B). The majority of the cross-peaks appeared in the range 7.8–8.4 p.p.m. for ^1H_N resonances and 108–123 p.p.m. for ^{15}N resonances in both cases. Most cross-peaks for PDCD5-(1–26) have chemical shifts identical with corresponding cross-peaks for PDCD5, except for the two terminal residues Gly^{25} and Asp^{26}. Cross-peak His^{21} showed slightly different chemical shifts in two spectra. The minor cross-peaks were observed for many residues of PDCD5-(1–26) in the two-dimensional ^{1}H-^{15}N HSQC spectrum (Figure 3A). The X-prolyl bond of Asp^{23}–Pro^{24} may result in the appearance of major and minor cross-peaks of remote residues in the sequence of PDCD5-(1–26). Side-chain resonance assignments for PDCD5-(1–26) were identified by comprehensive analysis of all homonuclear and heteronuclear multidimensional NMR data collected for PDCD5-(1–26).

The CSI (chemical shift index) derived from $^{13}C_\alpha$ and $^1H_\alpha$ chemical shifts for PDCD5-(1–26) is shown in Figure 4. A 'dense' group of positive secondary chemical shifts $\Delta^{13}C_\alpha$ was observed for residues Ser^1–Leu^{17}. Secondary chemical shifts Δ^1H_α provided negative values for all residues in sequence region Asp^3–Leu^{17} of PDCD5-(1–26). As has been indicated, $^{13}C_\alpha$ resonances of residues in α-helix experience a downfield shift of 2.0–4.0 p.p.m. compared with those in random coil, and $^1H_\alpha$ resonances shift upfield 0.15–0.60 p.p.m. [13,14]. Therefore the segment composed of residues Asp^3–Leu^{17} of PDCD5-(1–26) is supposed to form an α-helical structure.

Determination of α-helix structure of PDCD5-(1–26)

Sequential and medium-range NOE connectivities were identified for the sequence of PDCD5-(1–26) through d_{NN}, $d_{\alpha N}$, $d_{\alpha\beta}$ and $d_{\beta N}$ NOEs (Figure 5). PDCD5-(1–26) did not show any long-range NOE (more than five residues apart). The observed NOEs

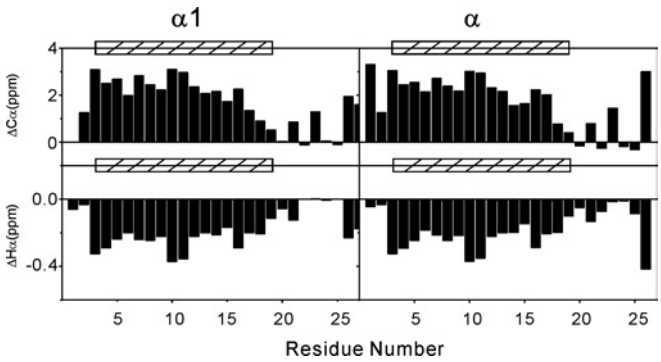

Figure 4 Secondary chemical shifts for $^{13}C_\alpha$ and $^{1}H_\alpha$ resonances of PDCD5-(1–26)

Secondary chemical shifts of PDCD5-(1–26) as a function of residue number (right panel). For comparison, the secondary chemical shifts for corresponding residues of human PDCD5 protein [4] are provided (left panel). The $\Delta^{13}C_\alpha$ and $\Delta^{1}H_\alpha$ values represent the chemical shift difference between those of the particular residues and the random coil values corrected by sequence [20,21].

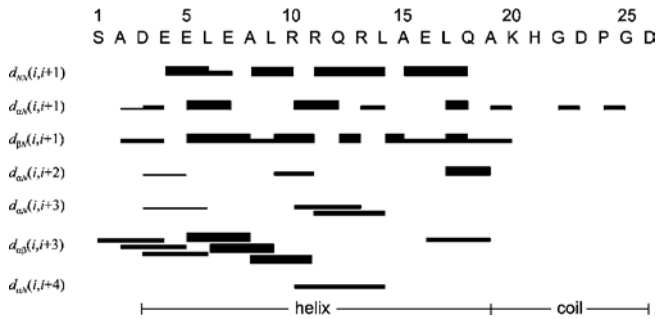

Figure 5 Summary of NOE connectivities obtained for PDCD5-(1–26)

The relative NOE intensities are indicated by the thickness of the bars, and the medium-range NOEs are indicated by lines connecting the two coupled residues.

represent the characteristic NOE connectivity features of an α-helix structure. The NOE connectivity together with the chemical shift index obtained for PDCD5-(1–26) provided a preliminary identification of the α-helix structure in the fragment.

Calculation of the structures was carried out using a total of 223 distance and 19 torsion angle restraints. Distance and dihedral angle restraints for structure determination and structure statistics of the 20 lowest energy structures from the family of 200 calculated structures are listed in Table 1. The superposition of 20 structures is shown in Figure 6(A). Validation of geometries of the 20 structures was performed using the program PROCHECK-NMR [15]. Ramachandran map analysis showed that the majority of the dihedral angles were in the most favoured regions (85.7 %) and none were in the disallowed regions (Table 1). The averaged R.M.S.D. (root mean square deviation) values for the segment involved in the α-helix structure were 0.23 ± 0.07 Å (1 Å = 0.1 nm) and 3.09 ± 0.96 Å for the backbone and all heavy atoms respectively, showing the well defined α-helix structure (Figures 6B and 6C).

Backbone dynamics of PDCD5-(1–26)

The values of the ^{1}H–^{15}N relaxation parameters, R_1, R_2 and NOE are shown in Figure 7. The overall pattern of variations in the R_1, R_2 and NOE values as a function of residue number are similar to each other. The sequence dependence of the relaxation parameters for residues in sequence region Asp^3–Ala^{19} are fairly constant; in particular, the R_2 and NOE values are generally smoother than R_1 values. The average values of R_1 and R_2 in this region are 3.34 ± 0.43 Hz and 5.36 ± 0.36 Hz respectively. The NOE values do not exceed the theoretical maximum, and the average value for residues Asp^3–Ala^{19} is 0.58 ± 0.14. The residues at the C-terminal region Lys^{20}–Asp^{26} have different relaxation features. A general decrease in the relaxation parameters occurs from residue Lys^{20}. Therefore residues Asp^3–Ala^{19} form a stable ordered α-helix structure, and residues in the tail region remain highly mobile.

Table 1 Distance and dihedral angle restraints for structural calculation and structure statistics for the family of 20 structures of PDCD5-(1–26)

vdw, van der Waals; 1 kcal = 4.184 kJ.

Parameter	Value
Number of distance restraints	
Total NOEs	223
Intraresidual NOEs	115
Sequential ($\|i-j\|=1$)	63
Medium range ($\|i-j\|<5$)	45
Long range ($\|i-j\|\geqslant 5$)	0
Dihedral angle restraints	
Φ angle	19
Ψ angle	19
CNS energies (kcal/mol):	
E_{total}	62.32 ± 0.91
E_{bond}	4.18 ± 0.11
E_{angle}	29.00 ± 1.04
E_{improp}	4.05 ± 0.24
E_{vdw}	17.63 ± 1.01
E_{NOE}	7.26 ± 0.19
PROCHECK_NMR Ramachandran map analysis	
Most favoured regions	85.7%
Additional allowed regions	9.5%
Generously allowed regions	4.8%
Disallowed regions	0%
R.M.S.D.s of backbone C′, N and C_α (Å)	
$\langle SA\rangle_\alpha$ versus $\langle \underline{SA}\rangle$	0.23 ± 0.15
$\langle SA\rangle_{total}$ versus $\langle \underline{SA}\rangle$	1.15 ± 0.15
R.M.S.D. s of all heavy atoms (Å)	
$\langle SA\rangle_\alpha$ versus $\langle \underline{SA}\rangle$	3.09 ± 0.96
$\langle SA\rangle_{total}$ versus $\langle \underline{SA}\rangle$	4.02 ± 1.08

Apoptosis triggered by PDCD5-(39–125) and intact PDCD5

A biochemical hallmark of apoptotic cell death is the translocation of PS (phosphatidylserine) from the cytoplasmic surface of the cell membrane to the external cell surface [16]. Exposure of PS at the surface of apoptotic cells is easily determined by flow cytometry using fluorescence-labelled annexin V, which specifically binds PS [17]. To determine the respective apoptotic effects of PDCD5-(39–125) and intact PDCD5, we detected cell PS exposure stained by annexin-V–FITC. As shown in Figure 8, the intact PDCD5 significantly enhanced the apoptosis of HL-60 cells induced by serum withdrawal. However, the effect on apoptosis-promoting of PDCD5-(39–125) is weaker than that of intact PDCD5. As a negative control, BSA had no effect on apoptosis-promoting of HL-60 cells induced by serum withdrawal. Since residues Lys^{20}–Glu^{38} of PDCD5 is a segment that connects the N-terminal α-helix and triple-helix bundle of PDCD5, weakening the effect on promoting cell apoptosis by PDCD5-(39–125) can be attributed to the deletion of the N-terminal α-helix in PDCD5.

DISCUSSION

Usually, peptides are shown to be flexible and have no ordered structure in solution owing to the lack of long-range interactions.

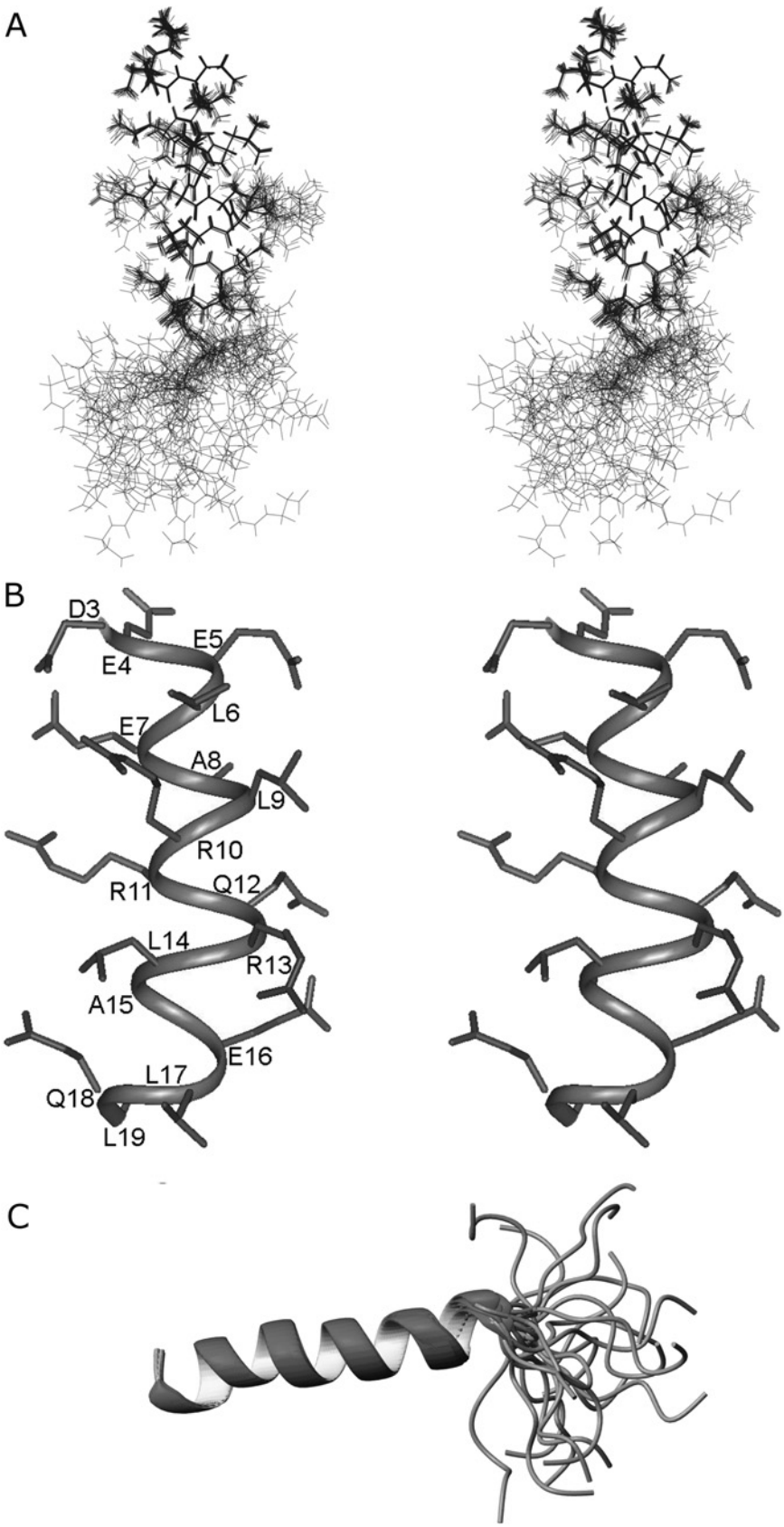

Figure 6 Solution structure of PDCD5-(1–26)

(**A**) A stereo view of superimposed 20 accepted solution structures of PDCD5-(1–26). (**B**) Stereo view shows the side-chains of residues Asp^{3}–Ala^{19} of PDCD5-(1–26). The heavy atoms of the side-chains are presented as sticks. (**C**) Ribbon presentation of α-helix structure of PDCD5-(1–26).

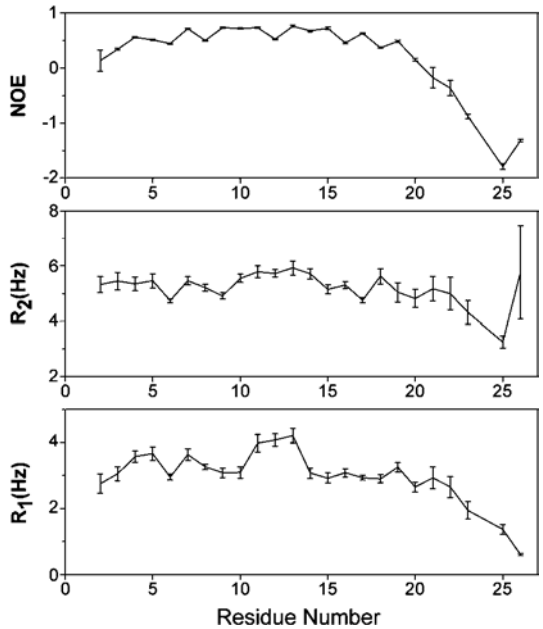

Figure 7 Relaxation rate constants R_1 and R_2 and steady-state NOE values for PDCD5-(1–26)

Errors were derived from the uncertainties of the least-squares fit to the exponential decay function (for R_1 and R_2) or from the signal-to-noise ratios (for NOE).

The N-terminal residues of PDCD5 do not provide any long-range NOE contacts with the residues in the main part of the protein [4]. However, a stable well-formed α-helix was determined for residues Asp^3–Ala^{19} of fragment PDCD5-(1–26), and the tail region consisting of residues Lys^{20}–Asp^{26} is flexible and unstructured. The similar secondary chemical shifts and distribution of cross-peaks in the two-dimensional ^{1}H–^{15}N HSQC spectra obtained for residues of PDCD5-(1–26) to those obtained for corresponding residues of PDCD5 (Figures 3 and 4) suggest that the N-terminal residues of PDCD5 can form a stable α-helix structure independently of the core of the protein.

The sequence region Asp^3–Ala^{19} of PDCD5-(1–26) contains four leucine residues, three alanine residues, and eight charged and two polar amino acid residues. Figure 9(A) shows a helical wheel construction of residues Asp^3–Ala^{19} in the α-helix. The helical wheel model reveals a symmetric distribution of the majority of residues for this α-helix structure. Paired residues Leu^{17}/Leu^6, Arg^{10}/Arg^{13}, Leu^{14}/Leu^9, Glu^7/Glu^{16}, and Ala^{15}/Ala^8, having identical amino acid type, are located symmetrically on the left and the right of the helical wheel in Figure 9(A). If we spread up the front and the back sides of the helix, as shown in Figure 9(B), we notice an interesting arrangement of the residues along the z-axis of the helix. In the sketched map for the front side of the helix, residues Glu^7, Arg^{10}, Agr^{13} and Glu^{16} of two paired residues Glu^7/Glu^{16} and Arg^{10}/Arg^{13} aligned along an oblique line downwards with the parallel alignment of four leucine residues, Leu^6, Leu^9, Leu^{14} and Leu^{17}, on both sides (left-hand

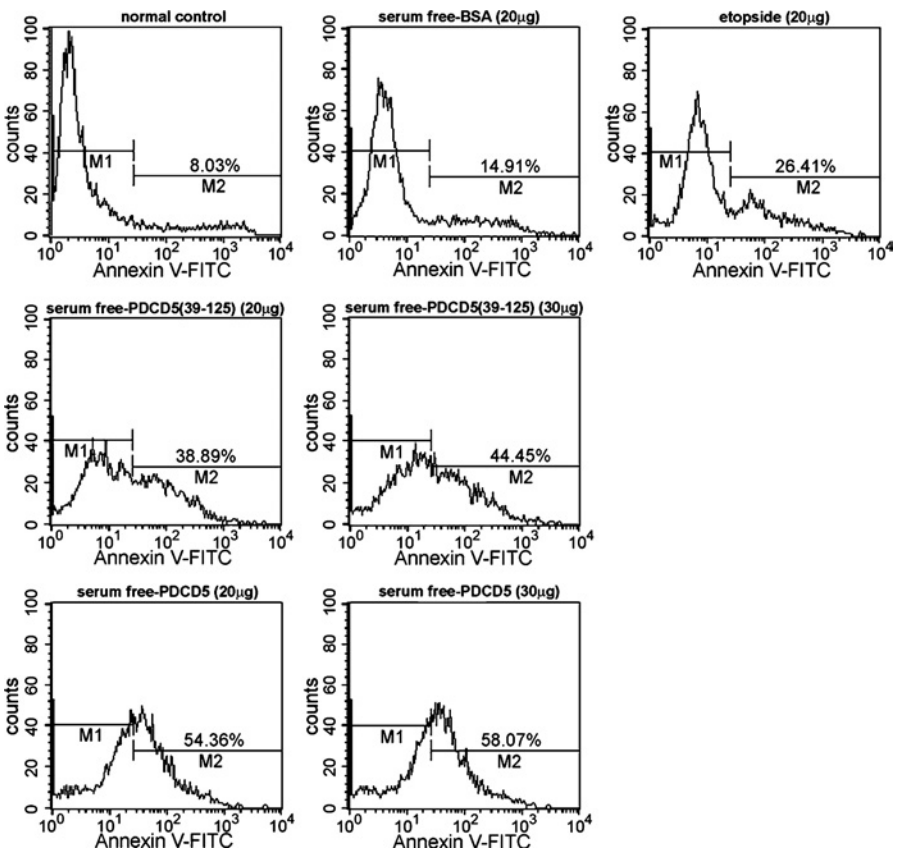

Figure 8 Flow cytometric analysis of HL-60 cells apoptosis induced by serum withdrawal

HL-60 cells were treated with a different amount of both PDCD5-(39–125) and intact PDCD5. Percentages of cell apoptosis were determined by flow cytometry with annexin-V–FITC. Numbers of M2 indicate the corresponding proportions of apoptotic cells that display positive annexin-V–FITC labelling. BSA and etoposide were used as negative and positive controls respectively. Experiments were performed in triplicate, with similar results.

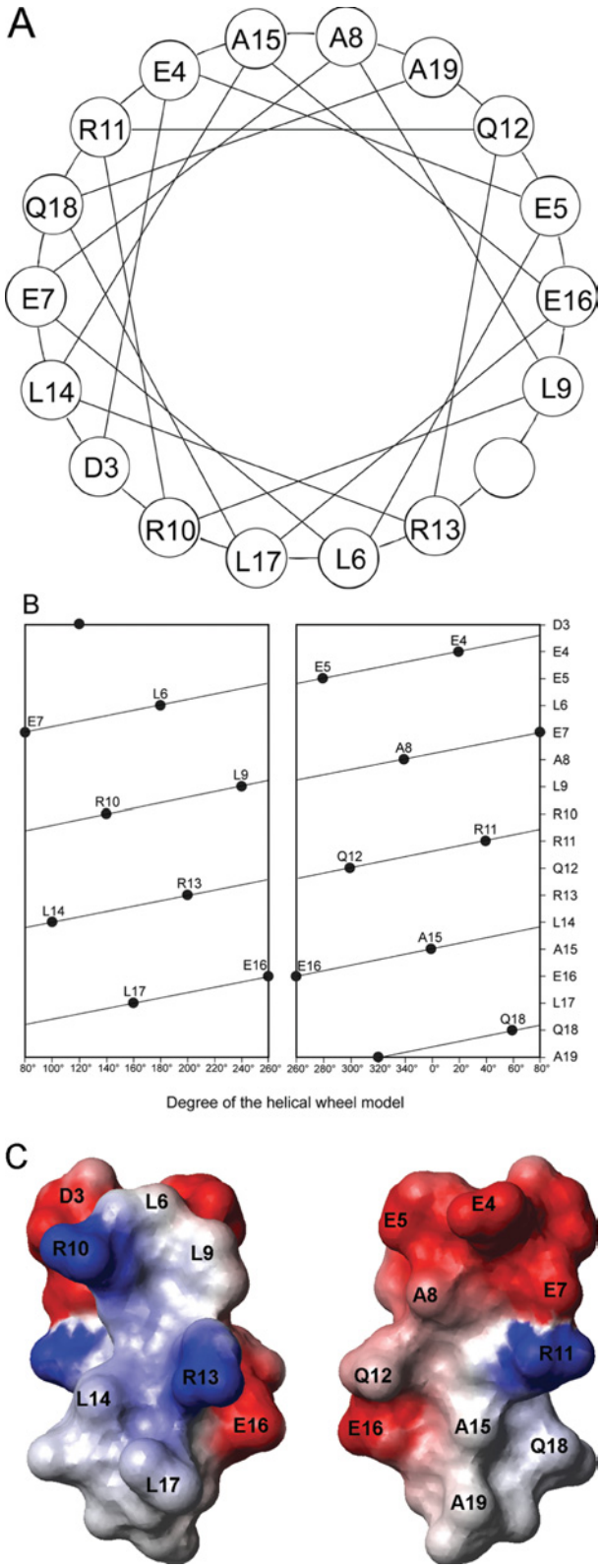

Figure 9 Surface character of helix formed by PDCD5-(1–26)

(**A**) Helical wheel model of residues Asp[3]–Ala[19] of PDCD5-(1–26) with NMR results taken into account. (**B**) Sketch maps showing the spread front (left-hand panel) and back (right-hand panel) sides of the helix. (**C**) Electrostatic potential surface of the helix calculated using MOLMOL [22]. The left-hand representation is the front face and the right-hand one is the back face of potential surface. The surface ionic groups are coloured from blue to red in accordance with the electrostatic charge from most positive to most negative.

panel, Figure 9B). The arrangement of Leu[6]/Arg[10]/Leu[14] and Leu[9]/Arg[13]/Leu[17] generates a characteristic hydrophobic/hydrophilic/hydrophobic potential surface of the front side of the helix (Figure 6B). On the spread back side of the helix, Ala[8] and Ala[15] aligned nearly parallel to the *z*-axis of the helix, with the hydrophilic residues, Glu[5], Gln[12] and Glu[16] on one side, and Glu[4], Glu[7], Arg[11] and Gln[18] on the other side (right-hand panel, Figure 9B). The back side of the helix provides a potential surface having hydrophilic/hydrophobic/hydrophilic character. In general, the back side of the helix has a surface that is more hydrophilic than the front side of the helix. Figure 9(C) shows the electrostatic potential surface on the front and back faces of the helix. Therefore the helix formed by PDCD5-(1–26) has a special character, which is different from the amphiphilic helical peptide. As is well known, the amphipathic character of amphiphilic helical peptide, defined as a α-helical domain containing opposite polar and non-polar 'face' [18], is found in many helices that are associated with plasma membrane. The plasma-membrane-associated helices may be either the *trans*-membrane or in-plane helices in the membrane bilayer [19].

Observation of the expression and localization of PDCD5 in the cell apoptosis process demonstrated the rapid translocation of PDCD5 to the nucleus of target cells undergoing apoptosis. The accumulation of PDCD5 in the nucleus precedes the chromosome DNA fragmentation and PS externalization [2]. However, how PDCD5 crosses the nuclear envelope and functions in the nucleus is still unclear. The N-terminal α-helix of PDCD5 has free orientation relating to the main part of the protein [4]. This may provide an environment for the N-terminal α-helix to serve as a functional entity independent of the PDCD5 protein. The apoptosis activity assay indicates that the deletion of the N-terminal α-helix of PDCD5 attenuates the apoptosis-promoting effects on HL-60 cells induced by serum withdrawal. This may correlate with different accumulations of PDCD5-(39–125) and intact PDCD5 in the nucleus. Thus it may be that the features of translocation of PDCD5-(39–125) and intact PDCD5 to the nucleus of cells are different. The N-terminal α-helix may play some role in the translocation of PDCD5 to the nucleus of target cells.

This research was supported by the National Natural Science Foundation of China (NNSFC 30170201), the 863 Special Program of China (Grant No. 2002BA711A13) and the Key Important Project from Chinese Academy of Sciences (Grant No. KSCX1-SW-17).

REFERENCES

1 Liu, H., Wang, Y., Zhang, Y., Song, Q., Di, C., Chen, G., Tang, J. and Ma, D. (1999) TFAR19, a novel apoptosis-related gene cloned from human leukemia cell line TF-1, could enhance apoptosis of some tumor cells induced by growth factor withdrawal. Biochem. Biophys. Res. Commun. **254**, 203–210

2 Chen, Y., Sun, R., Han, W., Zhang, Y., Song, Q., Di, C. and Ma, D. (2001) Nuclear translocation of PDCD5 (TFAR19): an early signal for apoptosis? FEBS Lett. **509**, 191–196

3 Wang, Y., Li, X., Wang, L., Ding, P., Zhang, Y., Han, W. and Ma, D. (2004) An alternative form of paraptosis-like cell death, triggered by TAJ/TROY and enhanced by PDCD5 overexpression. J. Cell Sci. **117**, 1525–1532

4 Liu, D., Feng, Y., Cheng, Y. and Wang, J. (2004) Human programmed cell death 5 protein has a helical-core and two dissociated structural regions. Biochem. Biophys. Res. Commun. **318**, 391–396

5 Christendat, D., Yee, A., Dharamsi, A., Kluger, Y., Savchenko, A., Cort, J. R., Booth, V., Mackereth, C. D., Saridakis, V., Ekiel, I. et al. (2000) Structural proteomics of an archaeon. Nat. Struct. Biol. **7**, 903–909

6 Feng, Y. M., Zhang, Y. M. and Jing, G. Z. (2002) Soluble expression in *Escherichia coli*, purification and characterization of a human TF-1 cell apoptosis-related protein TFAR19. Protein Expression Purif. **25**, 323–329

7 Hemsley, A., Arnheim, N., Toney, M. D., Cortopassi, G. and Galas, D. J. (1989) A simple method for site-directed mutagenesis using the polymerase chain reaction. Nucleic Acids Res. **17**, 6545–6551

8 Farrow, N. A., Muhandiram, R., Singer, A. U., Pascal, S. M., Kay, C. M., Gish, G., Shoelson, S. E., Pawson, T., Forman-Kay, J. D. and Kay, L. E. (1994) Backbone dynamics of a free and phosphopeptide-complexed Src homology 2 domain studied by ^{15}N NMR relaxation. Biochemistry **33**, 5984–6003
9 Zhu, G. and Bax, A. (1992) Improved linear prediction of damped NMR signals using modified "forward-backward" linear prediction. J. Magn. Reson. **100**, 202–207
10 Cavanagh, J., Fairbrother, W. J., Palmer, A. G. and Skelton, N. J. (1996) Protein NMR Spectroscopy, Academic Press, San Diego
11 Brunger, A. T., Adams, P. D., Clore, G. M., DeLano, W. L., Gros, P., Grosse-Kunstleve, R. W., Jiang, J. S., Kuszewski, J., Nilges, M., Pannu, N. S. et al. (1998) Crystallography & NMR system: a new software suite for macromolecular structure determination. Acta Crystallogr. Sect. D Biol. Crystallogr. **54**, 905–921
12 Thanabal, V., Omecinsky, D. O., Reily, M. D. and Cody, W. L. (1994) The ^{13}C chemical shifts of amino acids in aqueous solution containing organic solvents: application to the secondary structure characterization of peptides in aqueous trifluoroethanol solution. J. Biomol. NMR **4**, 47–59
13 Cornilescu, G., Delaglio, F. and Bax, A. (1999) Protein backbone angle restraints from searching a database for chemical shift and sequence homology. J. Biomol. NMR **13**, 289–302
14 Wishart, D. S., Sykes, B. D. and Richards, F. M. (1991) Relationship between nuclear magnetic resonance chemical shift and protein secondary structure. J. Mol. Biol. **222**, 311–333
15 Laskowski, R. A., Rullmannn, J. A., MacArthur, M. W., Kaptein, R. and Thornton, J. M. (1996) AQUA and PROCHECK-NMR: programs for checking the quality of protein structures solved by NMR. J. Biomol. NMR **8**, 477–486
16 Fadok, V. A., Bratton, D. L., Frasch, S. C., Warner, M. L. and Henson, P. M. (1998) The role of phosphatidylserine in recognition of apoptotic cells by phagocytes. Cell Death Differ. **5**, 551–562
17 Smith, J. D., Waelde, C., Horwitz, A. and Zheng, P. (2002) Evaluation of the role of phosphatidylserine translocase activity in ABCA1-mediated lipid efflux. J. Biol. Chem. **277**, 17797–17803
18 Motta, A., Pastore, A., Goud, N. A. and Castiglione Morelli, M. A. (1991) Solution conformation of salmon calcitonin in sodium dodecyl sulfate micelles as determined by two-dimensional NMR and distance geometry calculations. Biochemistry **30**, 10444–10450
19 Cross, T. A. and Opella, S. J. (1994) Solid-state NMR structural studies of peptides and proteins in membranes. Curr. Opin. Struct. Biol. **4**, 574–581
20 Schwarzinger, S., Kroon, G. J., Foss, T. R., Chung, J., Wright, P. E. and Dyson, H. J. (2001) Sequence-dependent correction of random coil NMR chemical shifts. J. Am. Chem. Soc. **123**, 2970–2978
21 Wishart, D. S., Sykes, B. D. and Richards, F. M. (1992) The chemical shift index: a fast and simple method for the assignment of protein secondary structure through NMR spectroscopy. Biochemistry **31**, 1647–1651
22 Koradi, R., Billeter, M. and Wüthrich, K. (1996) MOLMOL: a program for display and analysis of macromolecular structures. J. Mol. Graphics **14**, 51–55, 29–32

Received 27 April 2005/1 August 2005; accepted 5 August 2005
Published as BJ Immediate Publication 5 August 2005, doi:10.1042/BJ20050688